Journal of Energy Storage 60 (2023) 106589

Contents lists available at ScienceDirect

Journal of Energy Storage

journal homepage: www.elsevier.com/locate/est

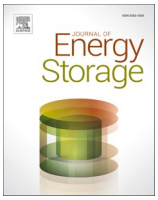

Research Papers

Investigation on the relations of operating parameters of a thermodynamic cycle energy storage system

Lisheng Pan [a,b,*], Yuehua Dong [a,b], Henglong Hao [a,b], Xuhui Zhang [b,c,**], Weixiu Shi [d], Xiaolin Wei [a,b]

[a] State Key Laboratory of High-temperature Gas Dynamics, Institute of Mechanics, Chinese Academy of Sciences, Beijing 100190, China
[b] School of Engineering Sciences, University of Chinese Academy of Sciences, Beijing 100049, China
[c] Key Laboratory for Mechanics in Fluid Solid Coupling Systems, Institute of Mechanics, Chinese Academy of Sciences, Beijing 100190, China
[d] Beijing Engineering Research Center of Sustainable Energy and Buildings, Beijing University of Civil Engineering and Architecture, Beijing 100044, China

ARTICLE INFO

Keywords:
Energy storage
CO_2 transcritical power cycle
CO_2 transcritical heat pump

ABSTRACT

In the background of carbon neutrality targets, energy for power generation is being converted from fossil to renewable sources. Energy storage has become particularly more and more important because it is a key technology to solve the instability of renewable energy. An energy storage method coupled with a heat pump and power cycle named thermodynamic cycle energy storage, which uses a heat pump and power cycle to run alternately for energy storage and has attracted the attention of international researchers because of its characteristics of green development, flexible application and convenience for large scale. The relations of operating parameters of the thermodynamic cycle energy storage are very important for operating this system sufficiently. Therefore, an optimization model of thermodynamic cycle energy storage was established for the CO_2 transcritical thermodynamic cycle, with hot water as a hot storage medium and NaCl brine as a cold storage medium. The relations of its operating parameters were analyzed by pinch point temperature difference and control variable method. The results showed that turning of some parameter curves occurs with changing the position of pinch point and largest temperature difference points. The round-trip efficiency generally increases firstly and then decreases with increasing the high-temperature side pressure of the power cycle. In the calculation range, when the evaporating pressure of the heat pump is 2.00 MPa, the high-temperature side pressure of the heat pump is 20.00 MPa, and the CO_2 temperature of the air cooler outlet is 20 °C, the peak value of round-trip efficiency is the largest, the maximum round-trip efficiency is 56.9 %.

1. Introduction

In order to deal with global ecological and environmental degradation, most countries and regions are planning to reach carbon neutrality by 2050. With people's higher and higher requirements for the comfort of life, the proportion of electricity in the terminal energy increased significantly [1]. In energy industry, especially the power generation industry, the degree of low-carbon development in the future is almost the key to realizing carbon neutrality [2]. Henze et al. [3] predicted that renewable energy generation will account for 84 % of total electricity generation by 2050, indicating the energy for power generation is being converted from fossil to renewable sources. Due to the strong dependence of renewable energy (mainly wind and solar energy) on climate, it is intermittent and volatile, leading to the instability of power generation [4], which makes it difficult to absorb, resulting in the phenomenon of abandoning wind and light. However, energy storage can reduce peak load and fill the valley, improve absorption capacity, avoid wind and light abandonment and improve energy utilization rate, which is an essential technical solution to solve the Spatio-temporal mismatch of energy resources in the future. Taking wind power generation as an example, the grid connection of 1 GW wind power generation requires a 200 MW standby power supply [5,6]. Therefore, a large-scale energy storage system as a standby power supply attracting more and more researchers' attention.

Based on the mechanism used, the types of energy storage system can

* Correspondence to: L. Pan, State Key Laboratory of High-temperature Gas Dynamics, Institute of Mechanics, Chinese Academy of Sciences, Beijing 100190, China.
** Correspondence to: X. Zhang, Key Laboratory for Mechanics in Fluid Solid Coupling Systems, Institute of Mechanics, Chinese Academy of Sciences, Beijing 100190, China.
E-mail addresses: panlisheng@imech.ac.cn (L. Pan), zhangxuhui@imech.ac.cn (X. Zhang).

https://doi.org/10.1016/j.est.2022.106589
Received 12 October 2022; Received in revised form 8 December 2022; Accepted 30 December 2022
Available online 7 January 2023

Nomenclature

c	specific heat capacity (kJ•kg^{-1}•°C^{-1})
C	mass concentration (kg•kg^{-1})
h	enthalpy (kJ•kg^{-1})
m	mass flow rate (kg•s^{-1})
p	pressure (MPa)
q	heat transfer at per unit mass flow of CO_2 (kW•kg^{-1})
Q	heat transfer at the actual mass flow rate of CO_2 (kW)
t	temperature (°C)
w	work done at per unit mass flow rate of CO_2 (kW•kg^{-1})
W	work done at the actual mass flow rate of CO_2 (kW)

Subscript

c	cold
com	compressor
cond	condenser
exp	expander
evap	evaporator
h	heat
high	system high-temperature side
HP	heat pump
low	system low-temperature side
PC	power cycle
pum	pump
RTE	round-trip efficiency
tur	turbine
isen	isentropy
max	maximum
1, 2, 3, 4, 5	state points of the transcritical cycle

Superscripts

'	inlet
"	outlet

Greek letters

Δt	temperature difference
η	efficiency
τ	duration

Abbreviation

COP	coefficient of performance
ODP	ozone-depleting potential

be classified into: electrochemical, chemical, electrical, thermal, and mechanical. Among them, electrochemical and mechanical energy storage are the most common in current types power grids, such as lead-acid batteries, flow batteries, pumped hydro energy storage, compressed air energy storage, flywheel energy storage, etc. [7,8]. Considering the characteristics of various energy storage technologies and the reasons for storage capacity, cost, charge and discharge efficiency, operation cost, environmental protection, etc., pumped hydro energy storage and compressed air energy storage [9,10] are recognized as typical large-scale (hundreds of MW or even GW) energy storage systems, and they all belong to mechanical energy storage. Pumped hydro energy storage is the most mature and widely used energy storage technology at present, but it is not suitable for general promotion in the period of the rapid growth of renewable energy installation due to its harsh site selection and long construction cycle. Compressed air energy storage mainly includes traditional compressed air energy storage and advanced adiabatic compressed air energy storage. The traditional compressed air energy storage for power generation requires fossil energy, and the gas storage chamber is generally a rock cave, abandoned mine, etc., which is limited by geographical conditions and cannot be flexibly applied [11]. Advanced adiabatic compressed air energy storage stores the heat of compressed air. Because the rise of compressed air temperature is relatively obvious and the temperature of the heat storage system is relatively high, the problem of a material's resistance to high temperature and high pressure needs to be solved, which also leads to high initial investment costs.

In 1924, German scholar of Marguerite [12] first proposed a system that converts electric energy into heat energy and then heat energy into electric energy. This system used water as a circulating working fluid and hot storage medium. In 1978, Cahn [13] changed the hot storage medium from water to hydrocarbon fraction on the above basis, and some current advanced adiabatic compressed air energy storage has used this kind of hot storage medium to store heat energy. In 2009, Hemrle et al. [14] proposed the basic model of thermodynamic cycle energy storage, which consists of two closed thermodynamic cycles. During the period of electricity abundance, electric energy is converted into thermal energy and cold energy through a heat pump and stored in the hot storage system and cold storage system, respectively. During the period of electricity shortage, the hot storage system is used as the high-temperature heat source and the cold storage system as the low-temperature heat source, and the heat energy is converted into electric energy through a power cycle. This thermodynamic cycle energy storage model can realize the mutual conversion between electric energy and heat energy through the heat pump and power cycle alternately operation. The overall structure of the thermodynamic cycle energy storage system is relatively compact, mainly including a compressor, expander, turbine, pump, heat exchanger and energy storage system, etc. In the same year, Hemrle et al. [15] also proposed a thermodynamic cycle energy storage model with an intermediate storage tank to optimize the heat transfer process at the high-temperature side. A shunt is set inside the gas heat exchanger to reduce the average heat exchange temperature difference between the circulating medium and the hot storage medium by controlling the mass flow of the hot storage medium. So as to improve the exergy efficiency of heat transfer and achieve the purpose of improving the round-trip efficiency.

In terms of working principle, all thermodynamic cycles, such as the Brayton cycle, Rankine cycle, transcritical thermodynamic cycle, and all circulating working fluids, such as CO_2, argon, and air, alkanes and their blend, can be adopted [16–18]. Because natural CO_2 has good thermodynamic properties, such as low critical point, high power density, low cost and zero ODP (Ozone Depletion Potential), researchers have also done a lot of theoretical and experimental work on CO_2 heat pump [19,20] and power cycle [21–23]. However, the analysis of the performance of a single cycle is no longer applicable to the energy storage system, because the energy storage system is coupled with a heat pump and power cycle.

In 2012, Mercangöz et al. [24] analyzed that the transcritical thermodynamic cycle was more conducive to improving the thermo-physical property matching degree between circulating working fluid and energy storage medium. A CO_2 transcritical thermodynamic cycle energy storage model with hot water as hot storage medium and saltwater as cold storage medium was established, and the analysis results showed that the maximum round-trip efficiency was 53 %. In 2012, Morandin et al. [25,26] proposed the heat storage principle of multiple storage tanks to improve round-trip efficiency and showed that the relations of some operating parameters were highly nonlinear. In order to find the optimal working conditions, the genetic algorithm was used to optimize the operating parameters of the thermodynamic cycle energy storage system and obtain the ideal hot water temperature curve, which requires the support of countless storage tanks. However, this is not realistic.

Through the least square method and piecewise linear fitting of the temperature curve of hot water, the parameters of the storage system of finite storage tank are obtained. The results showed that the maximum round-trip efficiency could reach 60 %. Further analysis by Morandin et al. [27] in 2013 showed that using an expander to replace the throttle valve for the CO_2 transcritical thermodynamic cycle energy storage increased the economic cost but could improve the round-trip efficiency of the system by more than 10 %. The Pareto optimal condition was obtained by selecting the system structure and operating parameters with a genetic algorithm to improve the system round-trip efficiency and reduce the investment cost. When the energy storage capacity was 50 MW, the round-trip efficiency could reach 64 %, and the corresponding investment cost was 684 $/kW. In 2013, Kim et al. [28] proposed an isothermal compression and isothermal expansion CO_2 transcritical thermodynamic cycle energy storage system, which has a higher back work ratio than the traditional isentropic compression and expansion system, so it is more conducive to improving round-trip efficiency. In 2014, Baik et al. [29] studied the influence of temperature of a low-temperature hot storage medium on the high-temperature side on round-trip efficiency by using a traditional CO_2 thermodynamic cycle energy storage system. It is shown that in order to maximize the round-trip efficiency of the CO_2 transcritical thermodynamic cycle energy system, it is necessary to optimize the temperature of the low-temperature hot storage medium at the high-temperature side. In 2016, Ayachi et al. [30] analyzed the CO_2 transcritical thermodynamic cycle energy storage system using stratum to store heat. They showed that when the minimum temperature difference between stratum and circulating working fluid for heat exchange increases from 1 °C to 5 °C, the round-trip efficiency decreases from 50 %–66 % to 42.5 %–55.5 %. In 2017, Wang et al. [31] reviewed and explored the thermodynamic cycle energy storage technology. The comparison with compressed air energy storage showed that the thermodynamic cycle energy storage system with CO_2 as a working medium has the advantages of a large energy storage scale, long working time, low investment cost and high cycle efficiency. In 2019, Reyes et al. [32] discussed the influence of introducing solar high-temperature heat on the performance of CO_2 transcritical thermodynamic cycle energy storage system. It showed that in the case of no solar support and a pressure ratio of 9.4, the round-trip efficiency is 52 %; in the case of solar support to improve the turbine inlet temperature, the round-trip efficiency is more than 60 %, and the turbine inlet temperature increases to 950 K at this time. In 2020, Liu et al. [33] proposed a creative liquid CO_2 energy storage system integrating the transcritical Brayton cycle, electrical thermal energy storage and ejector condensing cycle. The results showed that higher turbine inlet pressure and temperature can promote the net power output and round-trip efficiency of the system. The ejector entrainment ratio gives a decrease with the rise in ejector back pressure, and the decreasing trend is first steep until the ejector back pressure being at 8.2 MPa in the considered conditions and then becomes distinctly moderate. In 2021, Zhao et al. [34] optimized the thermal parameters of CO_2 transcritical thermodynamic cycle energy storage system with or without regenerator. The results showed that the energy storage system with regenerator has higher efficiency. When pressurized water is used as hot storage medium, the system efficiency without regenerator is 39.15 %, and the system efficiency with regenerator is 64.39 %. In 2022, Salomone-González et al. [35] analyzed a thermodynamic cycle energy storage system based on Rankie cycle and used different working fluids. Their model considered the main internal and external energy losses and heat leak to the environment. The results shows that when CO_2 is used as the working fluids, the cycle efficiency can reach 50 %.

To sum up, previous literature is devoted to optimizing the system structure to obtain the maximum round-trip efficiency and the lowest economic cost. However, the dependent relations of operating parameters between systems are not clear yet. CO_2 transcritical thermodynamic cycle energy storage system is a complex system with coupling with heat pump and power cycle, and the coupling relation has a significant impact on system performance. Therefore, it is necessary to study the dependent relation between operating parameters of CO_2 transcritical thermodynamic cycle energy storage system to fill the gaps in relevant research and provide a theoretical basis for the regulation and management of the system. In order to reveal the operation characteristics and influence mechanism of CO_2 transcritical thermodynamic cycle energy storage system, and obtain the universal rules of the energy storage system during operation. In this paper, a CO_2 transcritical thermodynamic cycle energy storage system model with hot water as the heat storage medium and NaCl brine as the cold storage medium was constructed. The pressure at the high-temperature side of the power cycle was discretized, and the relations between operating parameters of the CO_2 transcritical thermodynamic cycle energy storage system were analyzed and summarized by pinch point temperature difference [36] and control variable method.

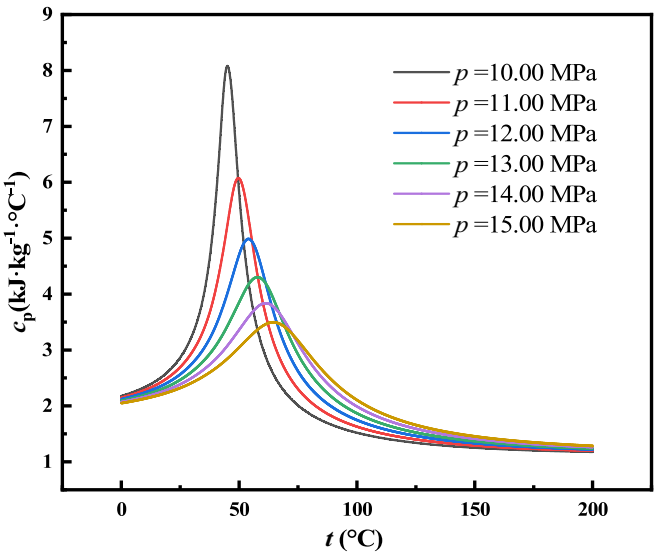

Fig. 1. Variation of specific heat capacity of supercritical CO_2 at constant pressure with the temperature under different pressures.

2. Methodology

2.1. Principle and model of CO_2 transcritical thermodynamic cycle energy storage

As shown in Fig. 1, in the supercritical state, the specific heat capacity of CO_2 at constant pressure changes significantly with temperature. In contrast, the specific heat capacity of liquid water is almost unchanged, resulting in poor heat transfer matching at the high-temperature side. As a result, the average temperature difference of heat transfer at the high-temperature side of the storage system is large, which reduces the reversibility of the thermodynamic cycle. Based on the existing research, the segmented heat transfer at the high-temperature side is considered to improve the matching degree of heat transfer at the high-temperature side.

The schematic diagram and optimization model diagram of the thermodynamic cycle energy storage system is shown in Fig. 2. This thermodynamic cycle energy storage system uses CO_2 as a circulating working fluid, hot water as a hot storage medium, and NaCl brine as a cold storage medium. This thermodynamic cycle energy storage system mainly includes a motor, generator, compressor, gas cooler (heater), expander, evaporator, condenser, turbine, pump, layered storage tank, storage tank, throttle valve, valve, pipeline, and other essential equipment.

It is worth noting that the layered storage tank diagram is divided into three layers, which is only a schematic diagram. In practical

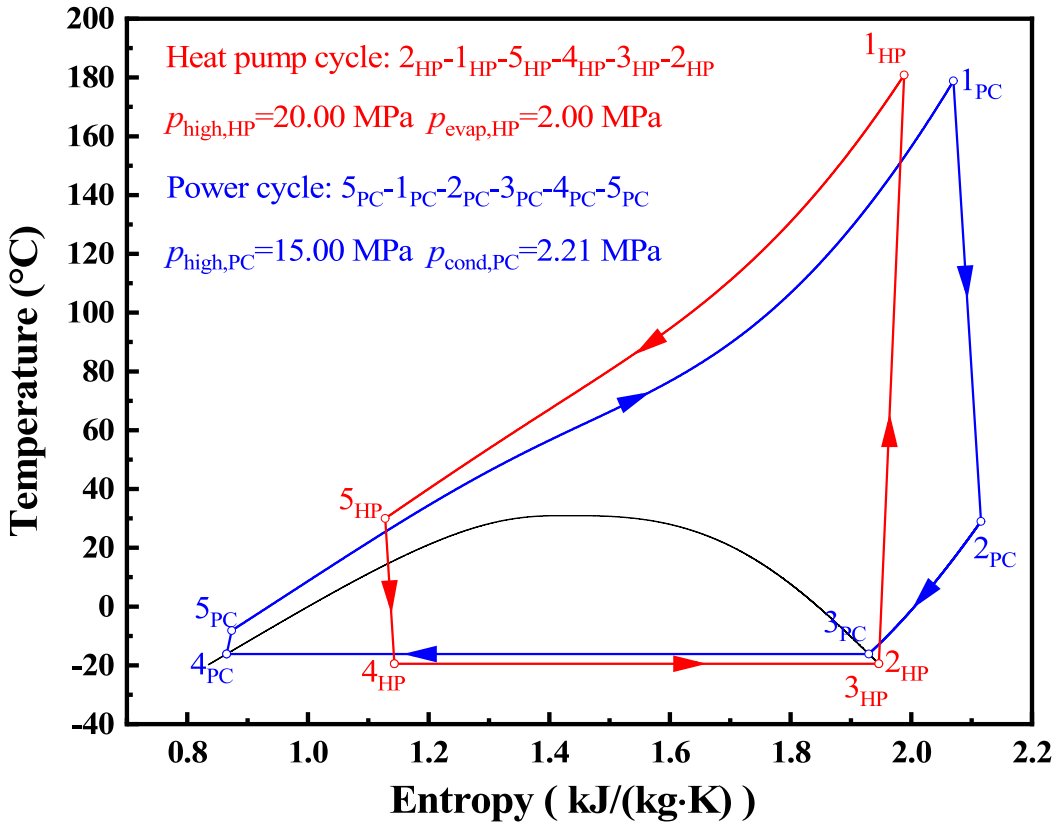

(a)

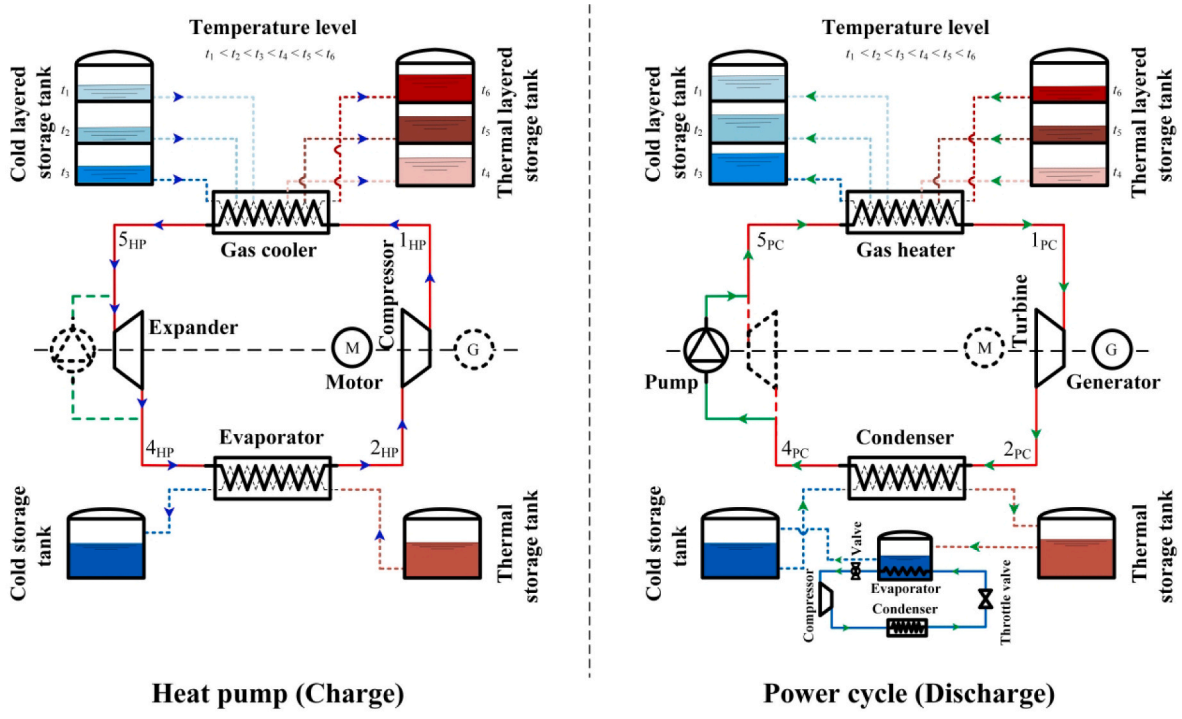

(b)

Fig. 2. Schematic diagram and optimization model diagram of CO_2 transcritical thermodynamic cycle energy storage (a: Schematic diagram; b: Optimization model diagram).

Table 1
Fixed parameters and study variable range.

Name	Value
Pinch point temperature difference (°C)	1.0
Inlet temperature difference of the heat pump evaporator (at 2_{HP}) (°C)	2.5
Compressor inlet superheat degree (°C)	0
Number of segments at high-temperature side	5
Auxiliary heat pump refrigeration coefficient	3
Isentropic efficiency of the compressor	0.88
Isentropic efficiency of the expander	0.90
Isentropic efficiency of the turbine	0.90
Isentropic efficiency of the pump	0.88
High-temperature side pressure of the power cycle (MPa)	10.00–30.00
Evaporating pressure of the heat pump (MPa)	2.00–3.00
High-temperature side pressure of the heat pump (MPa)	10.00–20.00
CO_2 temperature of the air cooler outlet (°C)	20.0–45.0

application, the number of layers in the storage tank is determined by the number of units of the heat exchanger.

During the period of electricity abundance, start the heat pump (2_{HP}-1_{HP}-5_{HP}-4_{HP}-3_{HP}-2_{HP}). The excess electric energy in the power grid is used to drive the motor, which drives the compressor to compress the low-temperature and low-pressure CO_2 (2_{HP}) from the evaporator into high-temperature and high-pressure gaseous CO_2 (1_{HP}). In the gas cooler, by controlling the mass flow rate of each layer of the left layered storage tank, according to the corresponding ways of high-temperature to high-temperature, moderate-temperature to moderate-temperature and low-temperature to low-temperature, high-temperature and high-pressure gaseous CO_2 heats the cold water from each layer of the left layered storage tank to hot water and stores it in the right layered storage tank. At the same time, gaseous CO_2 with high-temperature and high-pressure is cooled into gaseous CO_2 with low-temperature and high-pressure (5_{HP}). Then it expands into low-temperature and low-pressure CO_2 (4_{HP}) in the expander. The low-temperature and low-pressure CO_2 enters the evaporator to evaporate and absorb heat to become low-temperature and low-pressure CO_2 (2_{HP}) and finally enters the compressor to complete the cycle of the heat pump.

During the period of electricity shortage, start the power cycle (5_{PC}-1_{PC}-2_{PC}-3_{PC}-4_{PC}-5_{PC}). In the gas heater, by controlling the mass flow rate of each layer on the right layered storage tank, according to the corresponding ways of high-temperature to high-temperature, moderate-temperature to moderate-temperature, and low-temperature to low-temperature, the low-temperature and low-pressure liquid CO_2 from the pump (5_{PC}) is heated to high-temperature and high-pressure gaseous CO_2 (1_{PC}) by hot water from each layer of the layered storage tank at the right side. At the same time, the hot water is cooled to cold water and stored in a layered storage tank at the left side. Then the high-temperature and high-pressure gaseous CO_2 enters the turbine to expand for work and expands into low-temperature and low-pressure CO_2 (2_{PC}), which drives the generator to operate and generate electricity and is incorporated into the power grid. The low-temperature and low-pressure CO_2 enters the condenser and is cooled into liquid CO_2 (4_{PC}) by NaCl brine. Finally, the low-temperature and low-pressure liquid CO_2 is transported to the gas heater by pump to complete the power cycle.

In the case of only electric energy input without coupling other heat sources (such as industrial waste heat), the round-trip efficiency cannot reach 1 due to the irreversibility of the thermodynamic cycle, so part of electric energy will be dissipated in the form of heat energy. In order to maintain the thermal balance of the thermodynamic cycle energy storage system, a thermal balance system is set at the low-temperature side to extract the excess heat energy from the system. For the thermal balance system, as required, the NaCl brine at a higher temperature in the right side storage tank is drawn and cooled to a lower temperature (isothermal to the NaCl brine at the left side) and transferred to the left side storage tank. Due to the characteristics of the CO_2 transcritical thermodynamic cycle energy storage system's high pressure, the round-trip efficiency can be significantly improved by replacing the throttle valve with an expander [27]. However, the expander operates in the two-phase regions, which is harmful to the impeller. For the safe and reliable operation of the system, a non-impeller expander should be used, such as a piston expander, screw expander and so on [36].

2.2. Fixed parameters determination of thermodynamic cycle energy storage system

In theoretical analysis, according to the current manufacturing capacity of power machinery and heat exchanger, the following parameters of the thermodynamic cycle energy storage system are specified, as shown in Table 1. The pinch point temperature difference of heat exchanger is 5.0 °C. The inlet temperature difference of the heat pump evaporator (at 2_{HP}) is 5.5 °C. The compressor inlet superheat degree is 0 °C. The number of heat transfer units at the high-temperature side is 5. The auxiliary heat pump refrigeration coefficient is 3. The isentropic efficiency of the compressor, expander, turbine and pump are specified as 0.80, 0.75, 0.88 and 0.65, respectively [37]. Since the specific heat capacity at constant pressure of CO_2 varies significantly with temperature, the influence of pressure change at high-temperature side of the system is highly uncertain, so the pressure at high-temperature side of the power cycle is discretized. According to the practical application and the necessity of revealing the relations of operating parameters of thermodynamic cycle energy storage system, the following parameter ranges are specified in the theoretical calculation. The high-temperature side pressure of the power cycle range is 8.00–15.00 MPa. The evaporating pressure of the heat pump range is 1.75–3.00 MPa. The high-temperature side pressure of the heat pump range is 10.00–15.00 MPa. The CO_2 temperature of the air cooler outlet range is 20.0–45.0 °C.

The state point 3 in the heat pump and power cycle is all on the saturation gas line, which is not the actual running state point, but set for convenient analysis. In order to prevent the pump from not working properly due to its inlet being in the two-phase regions, the pump inlet (4_{PC}) is set on the saturated liquid line. The pressure drop of working fluid flow, mechanical efficiency of power machinery and heat dissipation loss of the system are not considered in the analysis.

It is worth noting that the isentropic efficiency of machinery, pinch point temperature difference of heat exchanger and refrigeration

Table 2
Comparison table of NaCl concentration and icepoint [38].

Mass concentration	Icepoint (°C)	Mass concentration	Icepoint (°C)	Mass concentration	Icepoint (°C)
0.00	0.00	0.09	−5.81	0.18	−14.05
0.01	−0.59	0.10	−6.56	0.19	−15.22
0.02	−1.19	0.11	−7.35	0.20	−16.46
0.03	−1.79	0.12	−8.18	0.21	−17.78
0.04	−2.41	0.13	−9.04	0.22	−19.18
0.05	−3.05	0.14	−9.94	0.23	−20.68
0.06	−3.70	0.15	−10.89	0.233	−21.13
0.07	−4.38	0.16	−11.89		
0.08	−5.08	0.17	−12.94		

Table 3
The specific heat capacity of ice varies with temperature [37].

Temperature (°C)	−40	−20	−10	0
Specific heat capacity of ice at constant pressure (kJ•kg^{-1}•°C^{-1})	1.821	1.947	2.010	2.060

coefficient of auxiliary heat pump system all affect the round-trip efficiency. The round-trip efficiency may be small or even negative, but this is a normal phenomenon. However, it will not affect the rule between system operating parameters.

2.3. Heat transfer calculation method of NaCl brine

2.3.1. Thermophysics of NaCl brine

Eutectic temperature is the temperature at which all salt and water in brine solidifies into eutectic, and the corresponding concentration of solution is called eutectic concentration. When the concentration of NaCl brine is lower than the eutectic concentration, the icepoint temperature of brine decreases with the increase of the concentration. Contrarily, with higher concentration than eutectic concentration, the icepoint temperature will increases with increasing the concentration. For NaCl brine, the eutectic temperature is −21.13 °C and the eutectic concentration is 23.3 %. The icepoint of NaCl brine with different concentrations is shown in Table 2.

The relation between icepoint temperature and concentration is obtained through a polynomial fitting, as shown in Eq. (1), where the sum of squares of fitting residuals is 2.32•10^{-4}.

$$t_{\text{icepoint}} = -6.87719\cdot10^{-4} - 58.72816\cdot C - 15.10368\cdot C^2 - 648.80085\cdot C^3 + 1521.78879\cdot C^4 - 4239.29187\cdot C^5 \tag{1}$$

where the unit of t_{icepoint} is °C, and C is the mass concentration of NaCl brine.

The specific heat capacity of liquid NaCl brine is related to mass concentration and temperature to a certain extent. Wu [39] used the polynomial fitting method to obtain the relations between the specific heat capacity of NaCl solution at constant pressure and mass concentration and temperature, as shown in Eq. (2), and pointed out that the maximum relative error is 0.83 % and the average relative error is 0.45 %.

$$\begin{aligned} c_{\text{p,brine}} &= 2.731 - 0.007194\cdot t + 7.284\cdot10^{-5}\cdot t^2 \\ &+56.54\cdot C + 0.1332\cdot t\cdot C - 2.2\cdot10^{-3}\cdot t^2\cdot C \\ &-8.418\cdot10^{2}\cdot C^2 - 0.3301\cdot t\cdot C^2 + 1.42\cdot10^{-2}\cdot t^2\cdot C^2 \\ &+5.1\cdot10^{3}\cdot C^3 - 2.289\cdot t\cdot C^3 - 2.652\cdot10^{-2}\cdot t^2\cdot C^3 \\ &-1.395\cdot10^{4}\cdot C^4 + 7.529\cdot t\cdot C^4 \\ &+1.419\cdot10^{4}\cdot C^5 \end{aligned} \tag{2}$$

where the unit of $c_{\text{p,brine}}$ is kJ•kg^{-1}•°C^{-1}, the unit of t is °C, and C is the mass concentration of NaCl brine.

The latent heat of solidification of water and melting of ice is 334 kJ•kg^{-1} [37], and the specific heat capacity of ice is shown in Table 3.

The formula of ice specific heat capacity changing with temperature is obtained by polynomial fitting, as shown in Eq. (3), where the sum of squares of residuals is 0.

$$c_{\text{p,ice}} = 2.06 + 0.00303\cdot t_{\text{ice}} - 2.3875\cdot10^{-4}\cdot t_{\text{ice}}^2 - 4.125\cdot10^{-6}\cdot t_{\text{ice}}^3 \tag{3}$$

where the unit of $c_{\text{p,ice}}$ is kJ•kg^{-1}•°C^{-1}, the unit of t_{ice} is °C.

2.3.2. Heat transfer calculation process and equivalent specific heat of NaCl brine

The condensing process of NaCl brine at icepoint temperature is shown in Fig. 3. In this process, heat is divided into three parts, one is sensible heat from high-temperature brine to low-temperature brine, the other is latent heat from liquid water in high-temperature brine to precipitate and freeze with the temperature decreases, and the last part is sensible heat from ice to further reduce the temperature, as shown in formula (4).

$$Q_{\text{all}} = Q_{\text{sensible,brine}} + Q_{\text{latent,ice}} + Q_{\text{sensible,ice}} \tag{4}$$

The calculation formula of brine mass concentration is shown in eq. (5).

$$C = \frac{m_{\text{brine,pure}}}{m_{\text{brine,pure}} + m_{\text{water}}} \times 100\% \tag{5}$$

where $m_{\text{brine,pure}}$ is the mass of pure NaCl in brine. The quality of water in brine can be obtained from eq. (5).

$$m_{\text{water}} = \left(\frac{1}{C} - 1\right)\cdot m_{\text{brine,pure}} \tag{6}$$

Therefore, the mass of water (ice) precipitated when the brine concentration increases C_{step} is shown in eq. (7).

$$m_{\text{ice}} = \left(\frac{1}{C} - \frac{1}{C + C_{\text{step}}}\right)\cdot m_{\text{brine,pure}} \tag{7}$$

The sensible heat $Q_{\text{sensible,brine}}$ from high-temperature brine to low-temperature brine is shown in Eq. (8).

$$Q_{\text{sensible,brine}} = \int_{t_{\text{brine,low}}}^{t_{\text{brine,high}}} c_{\text{p,brine}}\cdot m_{\text{brine}}\cdot \mathrm{d}t = \sum_{i=1}^{N\to\infty} c_{\text{p,brine}_i}\cdot m_{\text{brine}_i}\cdot\left(t_{\text{brine}_i} - t_{\text{brine}_{i-1}}\right) \tag{8}$$

The latent heat $Q_{\text{latent,ice}}$ of liquid water in high-temperature brine precipitates and freezes with the decrease of temperature is shown in eq. (9).

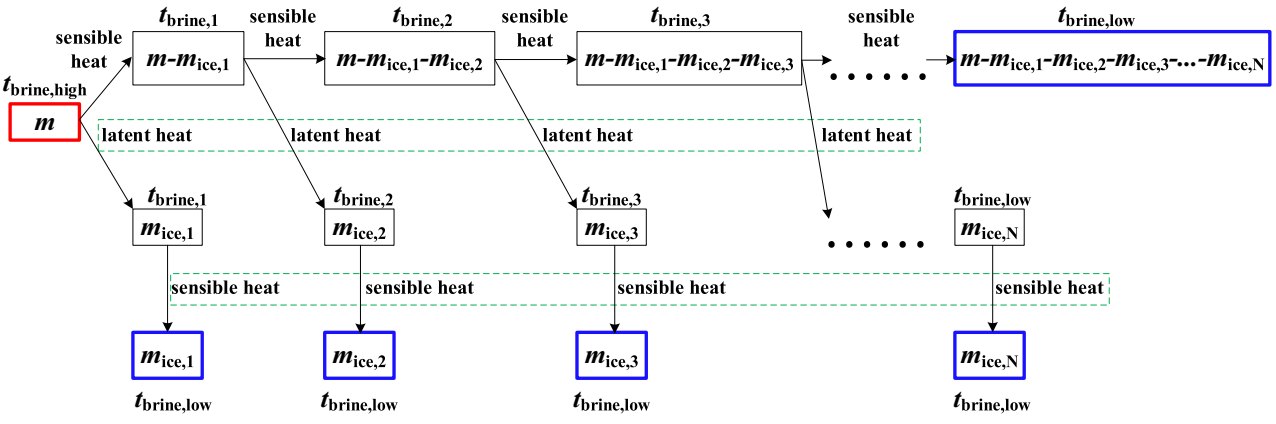

Fig. 3. Schematic diagram of NaCl brine condensing process.

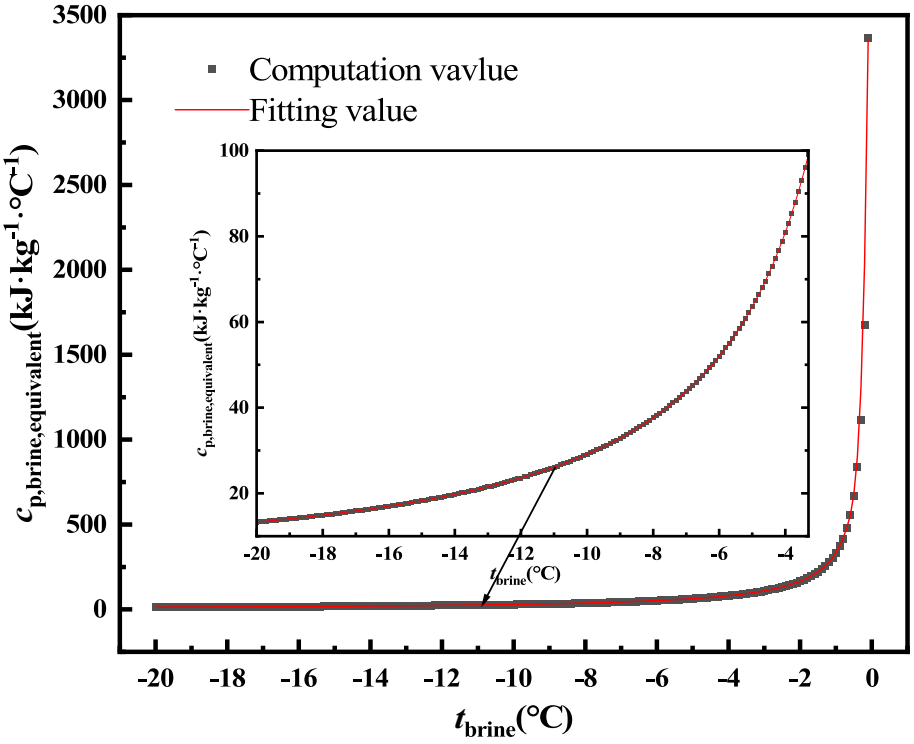

Fig. 4. Fitting curve of equivalent specific heat capacity of NaCl brine.

$$Q_{latent,ice} = \sum_{i=1}^{N} m_{ice_i} \cdot q_{latent} \tag{9}$$

where m_{ice_i} is the mass of ice shed each time, q_{latent} is the latent heat of solidification of water. m_{ice_i} is obtained from Eq. (7), as shown in Eq. (10).

$$m_{ice_i} = \left(\frac{1}{C_i} - \frac{1}{C_{i+1}}\right) \cdot m_{brine,pure} \tag{10}$$

The sensible heat $Q_{sensible,ice}$ of the shedding ice whose temperature decreases further is shown in Eq. (11).

$$Q_{sensible,ice} = \sum_{i=1}^{N} c_{p,ice_i} \cdot m_{ice_i} \left(t_{ice_i} - t_{brine,low}\right) \tag{11}$$

The equivalent specific heat capacity of NaCl brine is shown in Eq. (13).

$$c_{p,brine,equivalent} = \frac{Q_{all}}{m_{brine} \cdot \left(t_{brine,high} - t_{brine,low}\right)} \tag{13}$$

Through the above calculation method, the equivalent specific heat capacity of NaCl brine at icepoint temperature was calculated by taking a temperature rise of 0.001 °C, and the formula of the equivalent specific heat capacity of brine was fitted by three exponential function segments. The temperature range of brine was −20-0 °C, as shown in Eq. (14), and the piecewise fitting curve is shown in Fig. 4, where the sum of residual squares was 2619.46.

$$c_{p,brine,equivalent} \begin{cases} = 326.87 \cdot e^{t_{brine}/-0.976} + 142.10 \cdot e^{t_{brine}/-2.672} + 57.02 \cdot e^{t_{brine}/-8.917} + 7.14 \\ \qquad (-20^{\circ}C \le t_{brine} \le -3.3^{\circ}C) \\ = 1664.62 \cdot e^{t_{brine}/-0.185} + 730.72 \cdot e^{t_{brine}/-0.484} + 327.32 \cdot e^{t_{brine}/-1.842} + 43.65 \\ \qquad (-3.3^{\circ}C < t_{brine} \le -0.7^{\circ}C) \\ = 1784.10 \cdot e^{t_{brine}/-0.153} + 1784.10 \cdot e^{t_{brine}/-0.170} + 1784.10 \cdot e^{t_{brine}/-0.187} + 390.59 \\ \qquad (-0.7^{\circ}C < t_{brine} \le 0^{\circ}C) \end{cases} \tag{14}$$

To sum up, when the mass flow rate of brine is m_{brine}, NaCl brine with concentration C_{low} and temperature $t_{brine,high}$ at the icepoint is condensed into brine with concentration C_{high} and temperature $t_{brine,low}$ at the icepoint, and the heat Q_{all} released is shown in Eq. (12).

$$Q_{all} = \sum_{i=1}^{N\to\infty} c_{p,brine_i} \cdot m_{brine_i} \cdot \left(t_{brine_i} - t_{brine_{i-1}}\right) + \sum_{i=1}^{N\to\infty} m_{ice_i} \cdot q_{latent} + \sum_{i=1}^{N\to\infty} c_{p,ice_i} \cdot m_{ice_i} \left(t_{ice_i} - t_{brine,low}\right) \tag{12}$$

2.4. Calculation method for parameters of thermodynamic cycle energy storage system

The flow chart of calculation method for parameters of thermodynamic cycle energy storage system is shown in Fig. 5, including one main function and two sub-function.

For the heat pump, the state point 3_{HP} is obtained from the evaporating pressure. The compressor inlet parameters (state point 2_{HP}) can be obtained according to the set compressor inlet superheat degree. The compressor outlet parameter (state point 1_{HP}) can be obtained at the

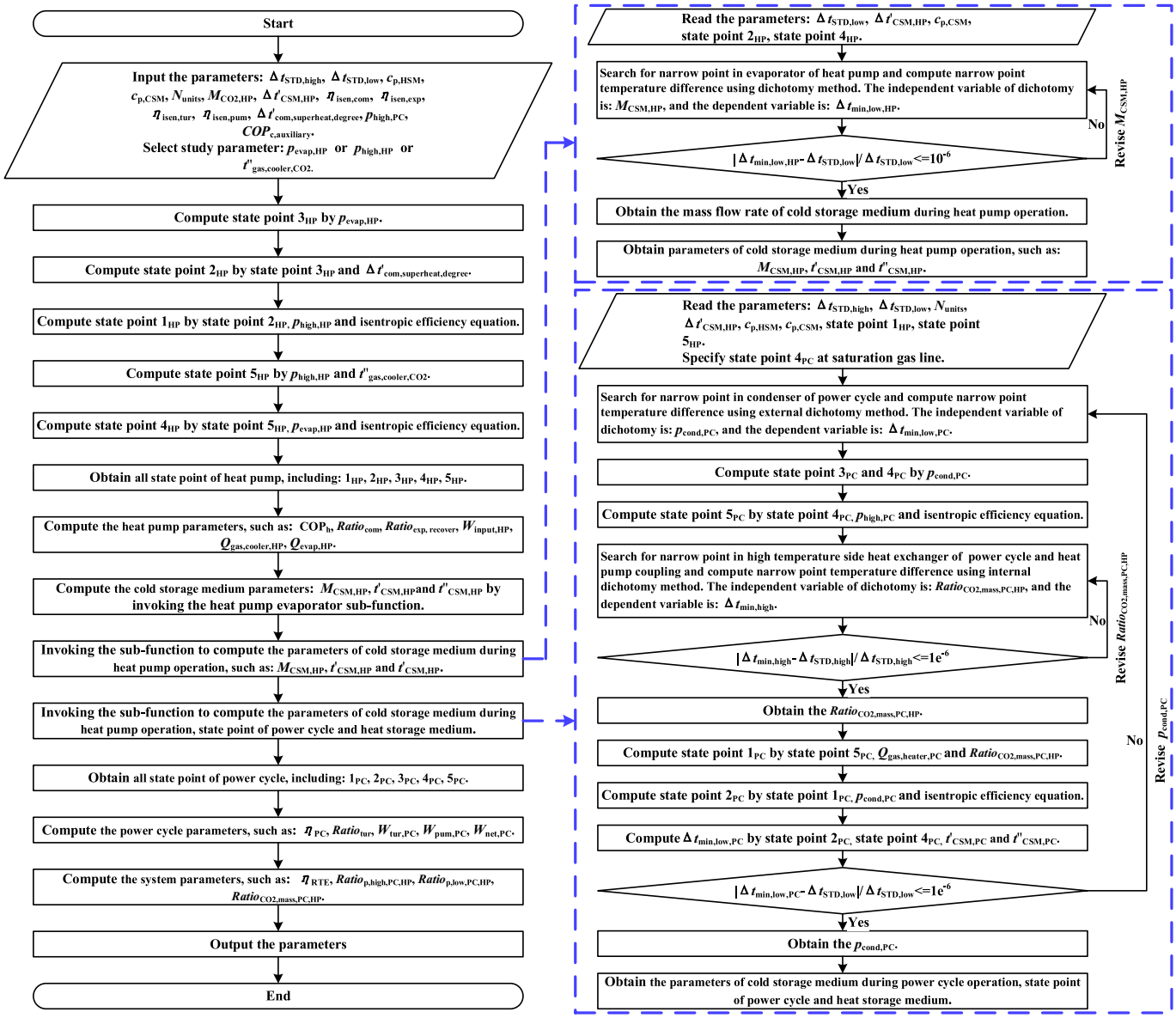

Fig. 5. Flow chart of calculation method for parameters of thermodynamic cycle energy storage system.

given high-temperature side pressure according to Eq. (15). The outlet parameters of the gas cooler (state point 5_{HP}) can be obtained by combining the CO_2 temperature of the gas cooler outlet with the pressure of the high-temperature side. According to Eq. (16), the expander outlet parameter (state point 4_{HP}) can be obtained. The mass flow rate and outlet temperature of cold storage medium are limited by the pinch point temperature difference of the evaporator, which can be solved by the pinch point temperature difference method according to the given inlet temperature difference of the evaporator (at 2_{HP}).

$$\eta_{isen,com} = \frac{h_{1,HP,isen} - h_{2,HP}}{h_{1,HP} - h_{2,HP}} \tag{15}$$

$$\eta_{isen,exp} = \frac{h_{5,HP} - h_{4,HP}}{h_{5,HP} - h_{4,HP,isen}} \tag{16}$$

Each state point of the heat pump is now known. Therefore, the compressor power consumption, expander power recovery, input electric energy, heat release to the high-temperature heat source and heat absorption from the low-temperature heat source at unit mass flow rate of CO_2 can be obtained by formula (17)–(21) below.

$$w_{com} = h_{1,HP} - h_{2,HP} \tag{17}$$

$$w_{exp} = h_{5,HP} - h_{4,HP} \tag{18}$$

$$w_{input,HP} = w_{com} - w_{exp} \tag{19}$$

$$q_{gas,cooler,HP} = h_{1,HP} - h_{5,HP} \tag{20}$$

$$q_{evap,HP} = h_{2,HP} - h_{4,HP} \tag{21}$$

For the power cycle, the inlet and outlet temperature of the cold storage medium has been determined. The condensing pressure at the low-temperature side of the power cycle should simultaneously satisfy the minimum temperature difference of heat transfer at the low-temperature side of the power cycle and the high-temperature side of coupling the heat pump and power cycle equal to the pinch point temperature difference. Therefore, an iterative calculation is required. According to the condensing pressure of the power cycle to be determined, state point 3_{PC} and pump inlet parameters (state point 4_{PC}) can be obtained. According to Eq. (22), the outlet parameters of pump (state point 5_{PC}) can be obtained. The ratio of the power cycle and heat pump CO_2

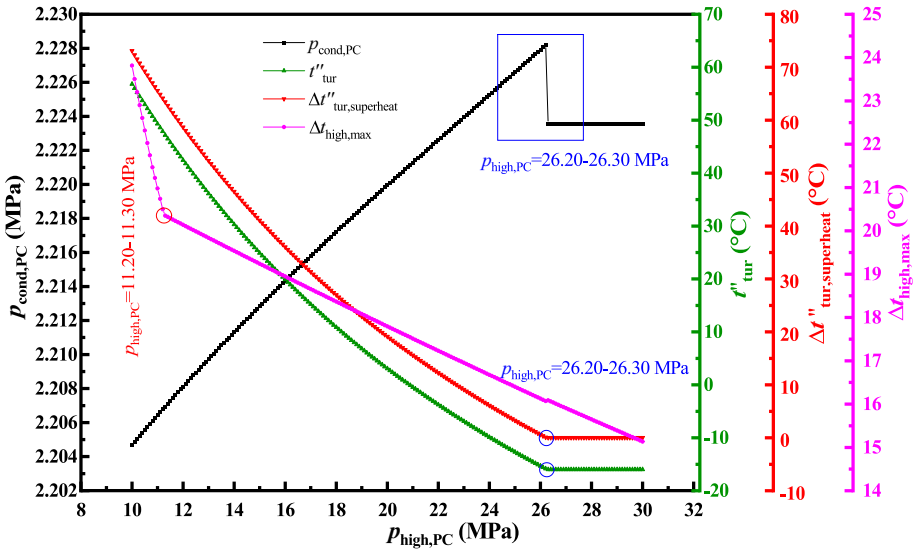

Fig. 6. Variation of $p_{cond,PC}$, t''_{tur}, $\Delta t''_{tur,superheat}$, $\Delta t''_{high,max}$ with high-temperature side pressure of the power cycle.

mass flow rate, the largest temperature difference of high-temperature side heat transfer, mass flow rate and inlet and outlet temperature of each unit of hot storage medium, and outlet parameters of gas heater (1_{PC}) can be obtained by pinch point temperature difference method. Then, the turbine outlet parameters (state point 2_{PC}) can be obtained according to Eq. (23). The mass flow rate of the cold storage medium is related to the position of the pinch point temperature difference at the low-temperature side of the power cycle, which is obtained by pinch point temperature difference method.

$$\eta_{isen,pum} = \frac{h_{5,PC,isen} - h_{4,PC}}{h_{5,PC} - h_{4,PC}} \tag{22}$$

$$\eta_{isen,tur} = \frac{h_{1,PC} - h_{2,PC}}{h_{1,PC} - h_{2,PC,isen}} \tag{23}$$

Each state point of the power cycle is now known. Therefore, the pump power consumption, the power done by turbine, the electric energy output and the heat released to the low-temperature heat source at unit mass flow rate of CO_2 can be obtained by formula (24)–(27) below.

$$w_{pum} = h_{5,PC} - h_{4,PC} \tag{24}$$

$$w_{tur} = h_{1,PC} - h_{2,PC} \tag{25}$$

$$w_{output,PC} = w_{tur} - w_{pum} \tag{26}$$

$$q_{cond,PC} = h_{2,PC} - h_{4,PC} \tag{27}$$

In fact, the power cycle and heat pump CO_2 mass flow ratio obtained in the above calculation is obtained when the running time of the power cycle and heat pump is the same. Nevertheless, the running time of the power cycle and heat pump is adjustable. The mass flow rate of hot storage medium and power cycle CO_2 can be adjusted in the same proportion according to the actual power generation and operation time, without affecting the size and position of the pinch point temperature difference.

If the heat pump running time is τ_{HP} and the power cycle running time is τ_{PC}, then:

$$W_{input,HP} = m_{CO_2,HP} \cdot w_{input,HP} \cdot \tau_{HP} \tag{28}$$

$$W_{output,PC} = m_{CO_2,PC} \cdot w_{output,PC} \cdot \tau_{PC} \tag{29}$$

$$Q_{balance} = m_{CO_2,PC} \cdot q_{cond,PC} \cdot \tau_{PC} - m_{CO_2,HP} \cdot q_{evap,HP} \cdot \tau_{HP} \tag{30}$$

$$W_{balance} = Q_{balance} / COP_{c,auxiliary} \tag{31}$$

$$W_{net,PC} = W_{output,PC} - W_{balance} \tag{32}$$

$$\eta_{RTE} = \frac{W_{input,HP}}{W_{net,PC}} \tag{33}$$

3. Results and discussion

Based on pinch point temperature difference and control variable method, the relations of operating parameters of the CO_2 transcritical thermodynamic cycle energy storage system have been analyzed. For the convenience of description and understanding, the following instructions should be noted in this study.

Instruction 1: "pinch point temperature difference position at the high-temperature side" refers to the position of the minimum temperature difference between heat pump CO_2 and hot storage medium or power cycle CO_2 and hot storage medium and in which heat transfer units (1–5). "largest temperature difference point position at the high-temperature side" refers to the maximum temperature difference between heat pump CO_2 and hot storage medium or power cycle CO_2 and hot storage medium and in which heat transfer units (1–5). The sequence of heat transfer units is from low-temperature to high-temperature.

Instruction 2: The turning caused by the position change of the pinch point temperature difference at the high-temperature side is called the first type of turning region. The turning caused by the position change of the largest temperature difference point at the high-temperature side is called the second type of turning region. The turning caused by the position change of the pinch point temperature difference at the low-temperature side of the power cycle from the saturated gas line to the turbine outlet is called the third type of turning region.

Instruction 3: In some cases, because the condensing pressure of the power cycle cannot simultaneously satisfy that the pinch point temperature difference at the high-temperature side is equal to the pinch point temperature difference, and the pinch point temperature difference at the low-temperature side of the power cycle is equal to the pinch point temperature difference and cannot be calculated, the previous working condition that cannot be calculated is defined as the termination working condition.

Instruction 4: The equivalent specific heat capacity of NaCl brine increases strongly with increasing its temperature, especially up to near 0 °C. In the iteration process of the pinch point, an exact calculation for

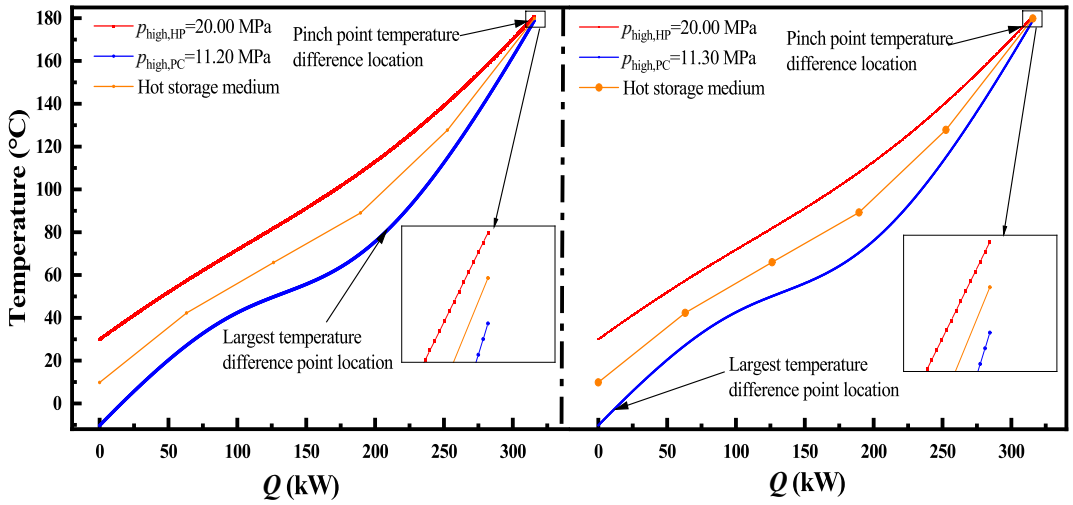

Fig. 7. Schematic diagram of largest temperature difference point position change at the high-temperature side.

the parameters of the pinch point is executed with many iterations of dichotomy. However, in the iteration process of the high temperature of the NaCl brine, its calculation accuracy can't reach as high as the parameters of the pinch point. Additionally, the large equivalent specific heat capacity of NaCl brine causes that the temperature varies slightly with temperature. Therefore, a little calculation error which is inevitable exists in the relative temperature between the pinch point temperature and the outlet temperature of the NaCl brine (in the condenser of the power cycle). Because of this reason, the pinch point temperature is a slightly higher than the outlet temperature of the NaCl brine (in the condenser of the power cycle) in some conditions and a peak value occurred for the condensing pressure of the power cycle.

Annotation instruction: The first type of turning region is marked with black circles and black words in the figure. The second type of turning region is marked by red circles and red words in the figure. The third type of turning region is marked with blue circles and blue words in the figure. Termination working condition is marked by a black square and black words in the figure. Due to the inevitable calculation error caused by the strongly increase of the specific heat capacity of the NaCl brine, the condensing pressure shows a peak phenomenon, marked by a blue square in the figure.

3.1. Analysis of curve turning region

Taking the evaporating pressure of the heat pump of 2.00 MPa, the high-temperature side pressure of the heat pump is 20.00 MPa, and the CO_2 temperature of the air cooler outlet is 30 °C as representative examples, the detailed analysis and interpretation of the curve turning region were carried out.

The variation of largest temperature difference of high-temperature side, condensing pressure of the power cycle, outlet temperature and outlet superheat degree of the turbine with high-temperature side pressure of the power cycle is indicated in Fig. 6. The curve turning region is shown in the figure. In the turning region of 11.20–11.30 MPa, the purple curve turn, which is the second type of turning region and is caused by the change of the position of the largest temperature difference point at the high-temperature side. A schematic diagram of largest temperature difference point position change at the high-temperature side is shown in Fig. 7. The position of the largest temperature difference point shifted from the fourth unit between power cycle CO_2 and hot storage medium to the first unit between power cycle CO_2 and hot storage medium, while the position of the pinch point temperature difference did not change at the fifth unit between power cycle CO_2 and hot storage medium. Under the high-temperature side pressure of the power cycle range of 26.20–26.30 MPa, the value of condensing

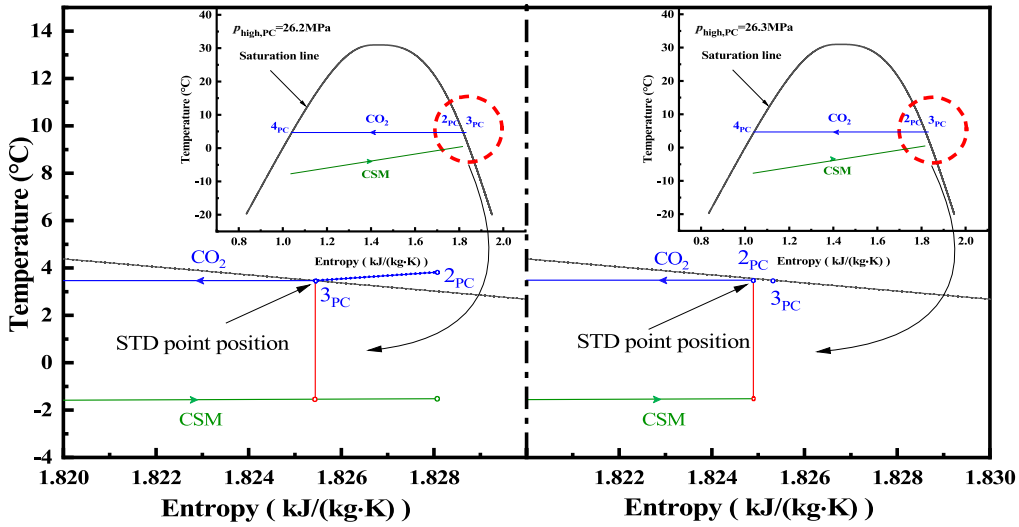

Fig. 8. Schematic diagram of pinch point temperature difference position change at the low-temperature side of the power cycle.

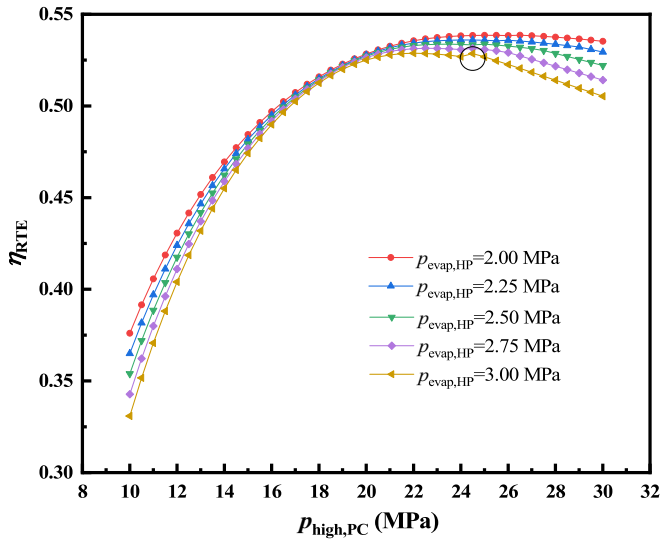

Fig. 9. Variation of round-trip efficiency with high-temperature side pressure of the power cycle under different evaporating pressures of the heat pump.

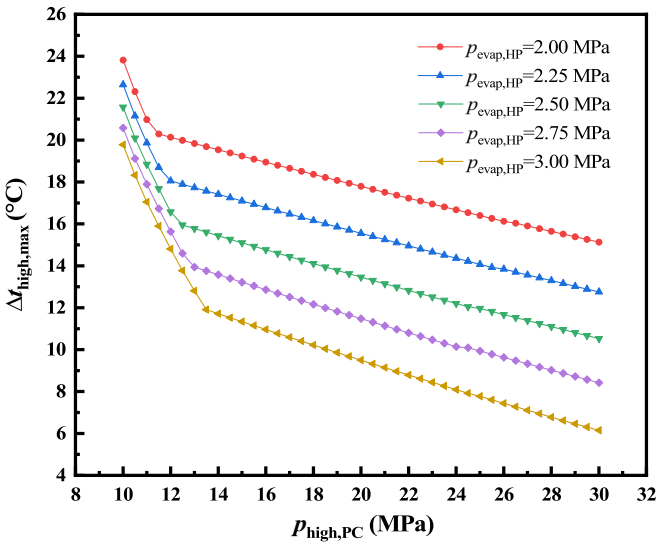

Fig. 10. Variation of the largest temperature difference of the high-temperature side with high-temperature side pressure of the power cycle under different evaporating pressures of the heat pump.

pressure of the power cycle, outlet temperature and outlet superheat degree of the turbine simultaneously occur a turning, which is the third type of turning region. The third type of turning region is caused by the position change of the pinch point temperature difference at the low-temperature side of the power cycle from the saturated gas line to the turbine outlet, as shown in Fig. 8. When the pressure at the high-temperature side of the power cycle is 26.20–26.30 MPa, the condensing pressure shows a peak due to the change of NaCl brine specific heat capacity, as shown in the blue box in Fig. 8. For details, see instruction 4.

It is also indicated from the Fig. 8 that after the third type of turning region, the condensing pressure, the outlet temperature and the superheat degree of the turbine all keep constant. The superheat degree at the exit of the turbine is 0 °C, which is consistent with the pinch point position at the low-temperature side of the power cycle in the two-phase region (turbine outlet). According to the characteristics of CO_2 saturation line, the increase of condensing pressure of the power cycle is conducive to the turbine outlet in the superheat region, and the lower the turbine outlet temperature is, the more conducive to the turbine outlet in the two-phase regions. Therefore, in the third type of turning region, the degree of increase of condensing pressure of the power cycle is less than the degree of decrease of turbine outlet temperature.

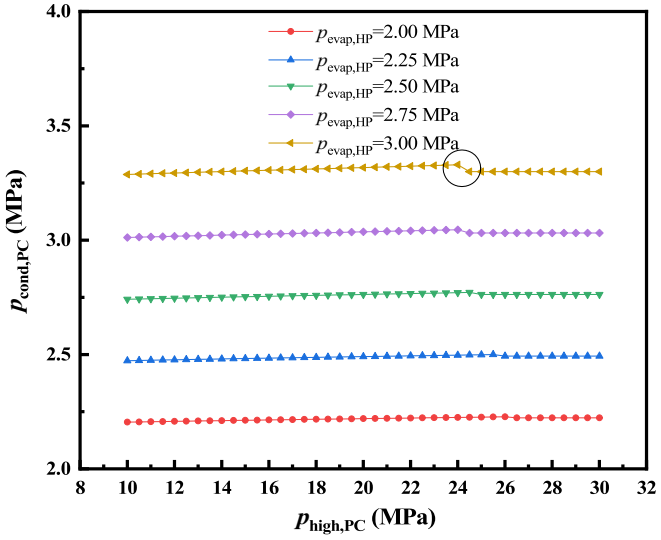

Fig. 11. Variation of condensing pressure of the power cycle with high-temperature side pressure of the power cycle under different evaporating pressures of the heat pump.

3.2. Influence of operating parameters

3.2.1. Influence of evaporating pressure of the heat pump

When analyzed the influence of evaporating pressure of the heat pump, the high-temperature side pressure of the heat pump is 20.00 MPa, and the CO_2 temperature of the air cooler outlet is 30 °C.

The variation of round-trip efficiency with high-temperature side pressure of the power cycle under different evaporating pressures of the heat pump is indicated in Fig. 9. From a horizontal perspective, with the increases of the high-temperature side pressure of the power cycle, the round-trip efficiency first increases and then decreases, and there is a peak value. From a longitudinal perspective, the round-trip efficiency decreases with the increase of evaporating pressure of the heat pump, and the peak position moves to the direction of the high-temperature side pressure of the power cycle decreases. The above analysis shows that when the evaporating pressure of the heat pump is constant, the proper high-temperature side pressure of the power cycle is helpful to improve the round-trip efficiency of the thermodynamic cycle energy storage system. When the high-temperature side pressure of the power cycle is constant, reducing the evaporating pressure of the heat pump is helpful to improve the round-trip efficiency. In the case of the evaporating pressure of the heat pump is 3.00 MPa, there is a non-derivable feature when the pressure at the high-temperature side of the power cycle is 24.00–24.50 MPa, as shown by the black circle in Fig. 9 and Fig. 11. It is caused by the change of the position of the largest temperature difference point and the position of the pinch point temperature difference at the high-temperature side at concurrent place.

Fig. 10 reflects the temperature difference level of the high-temperature side of the heat exchanger. The largest temperature difference at the high-temperature side first decreases rapidly, then decreases slowly with the increases of the high-temperature side pressure of the power cycle. In most cases, the decreases (increases) of the largest temperature difference at the high-temperature side will increases (decreases) the round-trip efficiency, which can represent the round-trip efficiency to a certain extent.

The variation of condensing pressure of the power cycle with high-

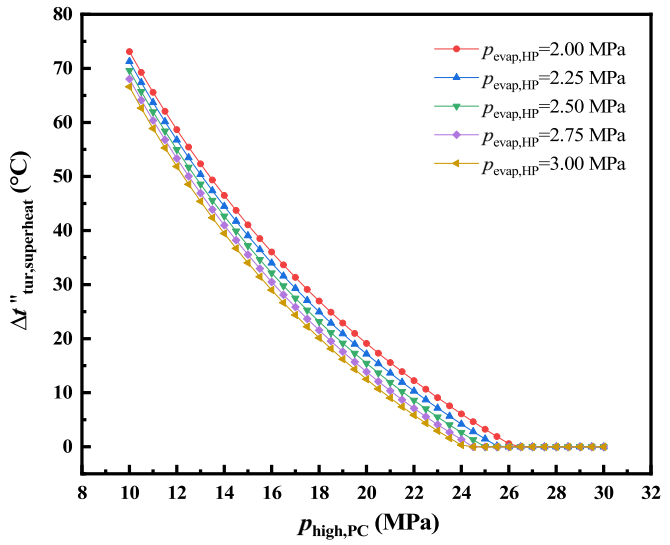

Fig. 12. Variation of turbine outlet superheat degree with high-temperature side pressure of the power cycle under different evaporating pressures of the heat pump.

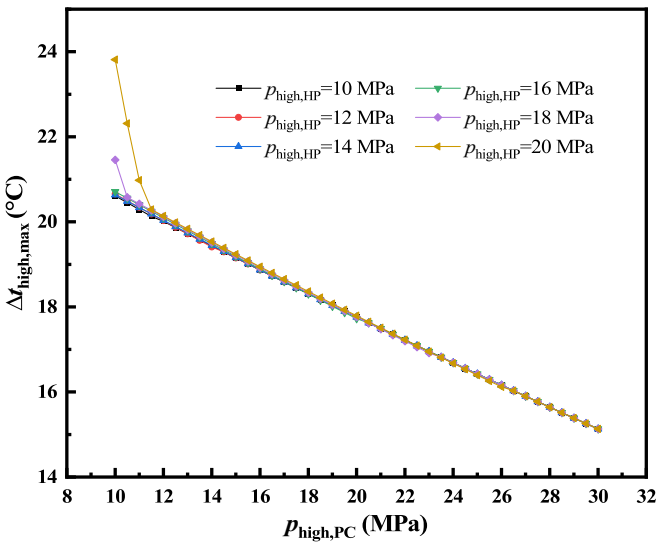

Fig. 14. Variation of the maximum temperature difference of heat transfer on the high-temperature side with high-temperature side pressure of the power cycle under different high-temperature side pressures of the heat pump.

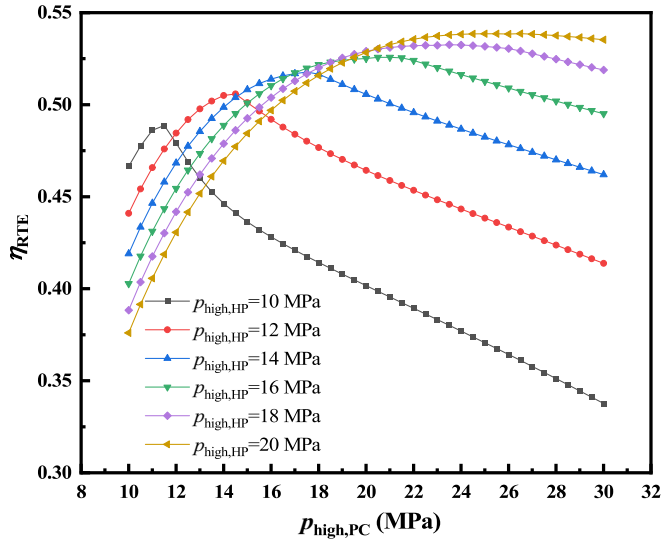

Fig. 13. Variation of round-trip efficiency with high-temperature side pressure of the power cycle under different high-temperature side pressures of the heat pump.

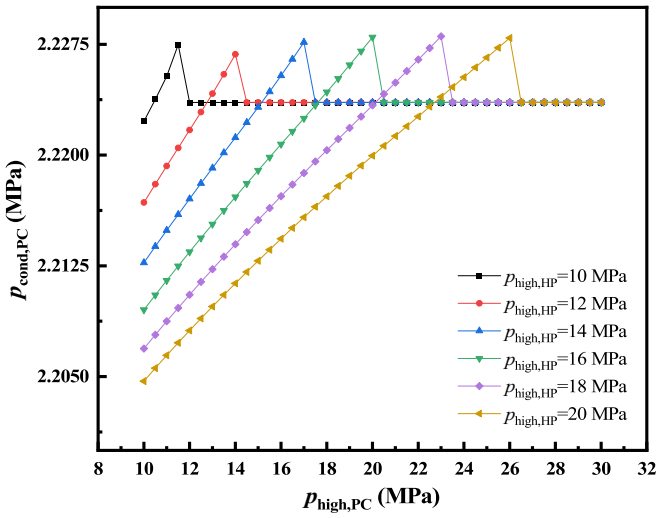

Fig. 15. Variation of condensing pressure of the power cycle with high-temperature side pressure of the power cycle under different high-temperature side pressures of the heat pump.

temperature side pressure of the power cycle under different evaporating pressures of the heat pump is indicated in Fig. 11. When the evaporating pressure of the heat pump is between 2.00 and 3.00 MPa, from a horizontal perspective, with the increases of the pressure at the high-temperature side of the power cycle, the condensing pressure of the power cycle basically remains unchanged. From a longitudinal perspective, with the increases of the evaporating pressure of the heat pump, the condensing pressure of the power cycle increases.

The variation of turbine outlet superheat degree with high-temperature side pressure of the power cycle under different evaporating pressures of the heat pump is indicated in Fig. 12. From a horizontal perspective, with the increases of the pressure at the high-temperature side of the power cycle, it decreases more and more slowly and finally keeps a constant value of zero (the turbine outlet enters the two-phase regions). From a longitudinal perspective, with the evaporating pressure of the heat pump increases, on the one hand, the superheat degree of the turbine outlet decreases before keeping constant value, on the other hand, they all finally enter the two-phase regions, and the position of turbine outlet enters the two-phase region moves in the direction of decreasing the high-temperature side pressure of the power cycle. Therefore, in order to maintain the normal operation of the turbine, it is necessary to avoid the situation that the high-temperature side pressure of the power cycle is too high, so as to avoid the turbine outlet in the two-phase regions.

3.2.2. *Influence of high-temperature side pressure of the heat pump*

When analyzed the influence of the high-temperature side pressure of the heat pump, the evaporating pressure of the heat pump is 2.00 MPa, and the CO_2 temperature of the air cooler outlet is 30 °C.

As shown in Fig. 13, for the high-temperature side pressures of the heat pump between 10.00 and 20.00 MPa, the trend of curves change is roughly the same. With the increase of the high-temperature side pressure of the heat pump, the peak value moves to the direction of increasing high-temperature side pressure of the power cycle, and the peak value becomes larger and larger. Therefore, when the high-

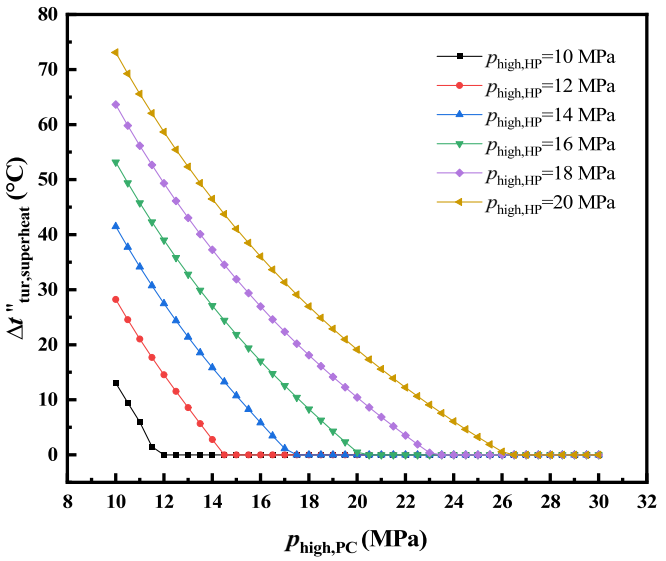

Fig. 16. Variation of turbine outlet superheat degree with high-temperature side pressure of the power cycle under different high-temperature side pressures of the heat pump.

temperature side pressure of the heat pump is constant, the selection of appropriate high-temperature side pressure of the power cycle can maximize the round-trip efficiency of the thermodynamic cycle energy storage system.

The variation of the largest temperature difference of the high-temperature side with high-temperature side pressure of the power cycle under different high-temperature side pressures of the heat pump is indicated in Fig. 14. From a horizontal perspective, with the increase of the high-temperature side pressure of the power cycle, it firstly decreases rapidly and then decreases slowly. From a longitudinal perspective, the turning point value moves in the direction of increasing pressure of the high-temperature side of the power cycle.

Fig. 15 illustrates the variation of condensing pressure of the power cycle with high-temperature side pressure of the power cycle under different high-temperature side pressures of the heat pump. From a horizontal perspective, with the increases of the high-temperature side pressure of the power cycle, the condensing pressure of the power cycle shows a general trend of steadily increasing first, then keeping constant. The reasons for the peak are detailed in Instruction 4. From a longitudinal perspective, with the increases of the high-temperature side pressure of the heat pump, on the one hand, before remaining unchanged, the higher the high-temperature side pressure of the heat pump, the lower the condensing pressure of the power cycle, on the other hand, the constant values at last are all equal and the position of entering constant value region move to the direction of the high-temperature side pressure of the power cycle increase.

As shown in Fig. 16, for the high-temperature side pressures of the heat pump between 10.00 and 20.00 MPa, from a horizontal perspective, with the increases of the high-temperature side pressure of the power cycle, it first decreases, then keeps a constant value of zero (the turbine outlet enters the two-phase regions). From a longitudinal perspective, with the increases of high-temperature side pressure of the heat pump, on the one hand, before keeping constant value, the turbine outlet superheat degree increases, on the other hand, the constant value position moves to the direction of increasing high-temperature side pressure of the power cycle. This is consistent with the phenomenon described in Fig. 15 that the constant value is finally maintained with the increase of the high-temperature side pressure of the power cycle, indicating that the turbine outlet enters the two-phase regions.

3.2.3. *Influence of CO_2 temperature of the air cooler outlet*

When analyzed the influence of CO_2 temperature of the air cooler outlet, the evaporating pressure of the heat pump is 2.00 MPa, and the high-temperature side pressure of the heat pump is 20.00 MPa.

As shown in Fig. 17, from a horizontal perspective, with the increases of the high-temperature side pressure of the power cycle, all curves show a trend of first increases and then decreases and there is a peak value.

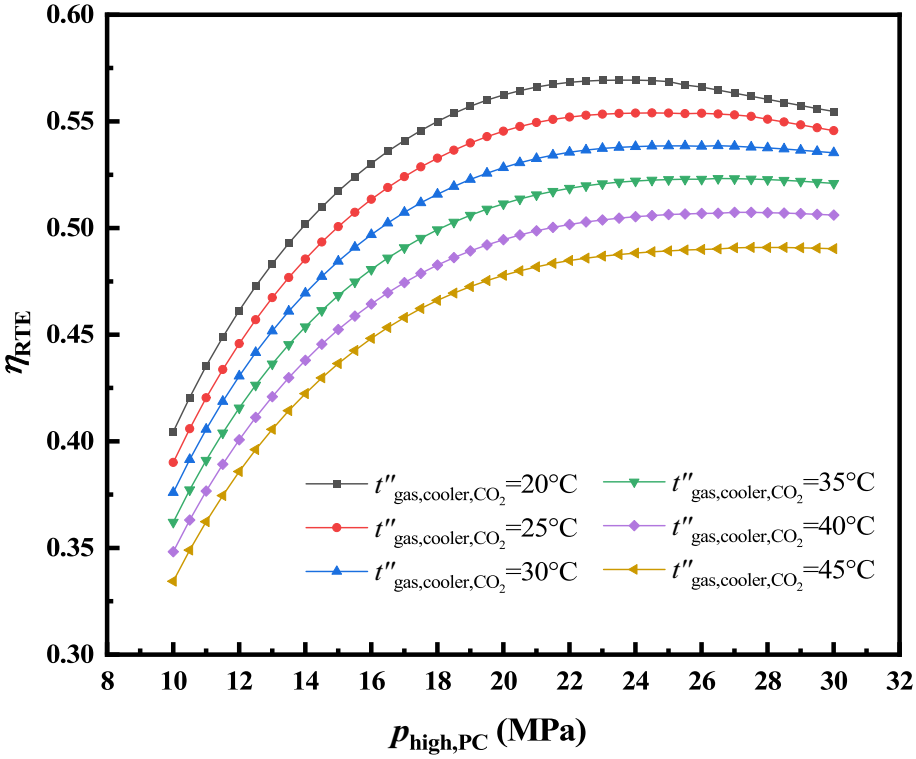

Fig. 17. Variation of round-trip efficiency with high-temperature side pressure of the power cycle under different CO_2 outlet temperatures of air cooler.

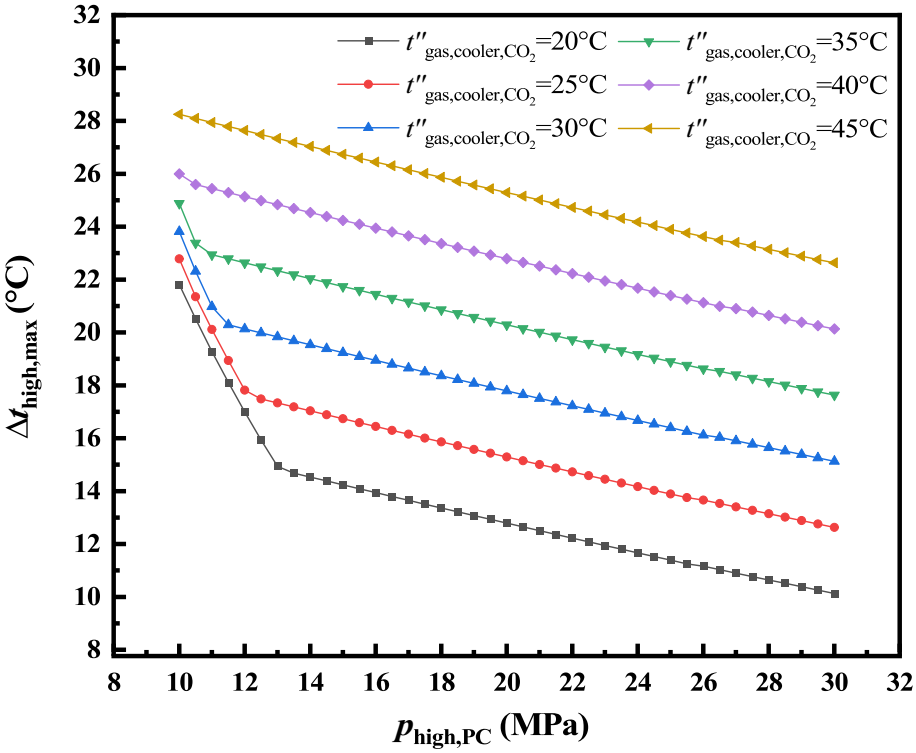

Fig. 18. Variation of the largest temperature difference of the high-temperature side with the high-temperature side pressure of the power cycle under different CO_2 temperatures of the air cooler outlet.

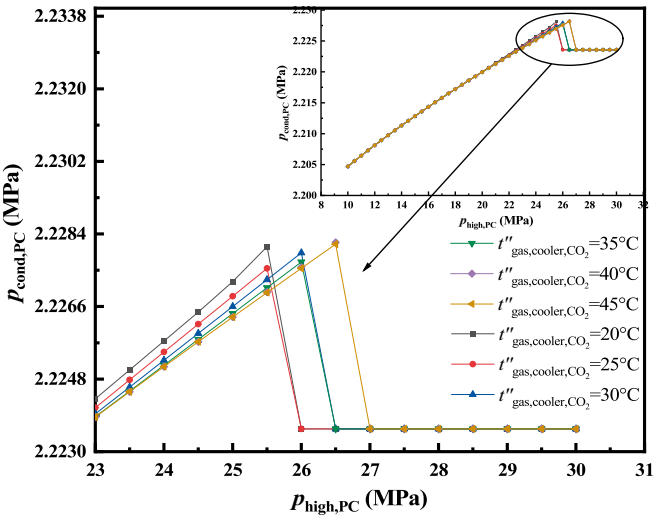

Fig. 19. Variation of condensing pressure of the power cycle with high-temperature side pressure of the power cycle under different CO_2 temperatures of the air cooler outlet.

From a longitudinal perspective, the peak value decreases with the increases of the CO_2 temperature of the air cooler outlet, and the position of the peak value moves to the direction of the increasing of the high-temperature side pressure of the power cycle. In the calculation range, when the CO_2 temperature of the air cooler outlet is 20 °C, the peak value of round-trip efficiency is the largest.

The variation of the largest temperature difference of the high-temperature side with the high-temperature side pressure of the power cycle under different CO_2 temperatures of the air cooler outlet is indicated in Fig. 18. When the outlet temperature of the air cooler is between 20 and 45 °C, it decreases rapidly first and then slowly. From a longitudinal perspective, the turning point value moves in the direction of increasing pressure of the high-temperature side of the power cycle. However, when the CO_2 temperatures of the air cooler outlet are 45 °C, it decreases slowly from beginning to end.

Fig. 19 shows the variation of condensing pressure of the power cycle with high-temperature side pressure of the power cycle under different CO_2 temperatures of the air cooler outlet. For the circumstance that the CO_2 temperatures of the air cooler outlet are between 20 and 45 °C, from a horizontal perspective, with the increases of the high-temperature side pressure of the power cycle, the curves of different CO_2 temperatures of the air coolers outlet coincide with each other in the slowly increasing region. From a longitudinal perspective, with the increases of the CO_2 temperature of the air cooler outlet, the condensing pressure of the power cycle becomes smaller and smaller in the fastly increasing region, and the position of exits the slowly increasing region and enters the constant value region moves in the direction of the increases of the high-temperature side pressure of the power cycle. It is worth noting that the condensing pressure at the low-temperature side of the power cycle is the same when the final remains constant.

Fig. 20 illustrates the variation of turbine outlet superheats degree with high-temperature side pressure of the power cycle under different CO_2 temperatures of the air cooler outlet. For the CO_2 temperatures of the air cooler outlet are between 20 and 45 °C, from a horizontal perspective, with the increases of the high-temperature side pressure of the power cycle, it shows a trend of decreasing and then keeps a constant value of zero (the turbine outlet enters the two-phase regions). From a longitudinal perspective, in the high-temperature side pressure are between 22 and 30 MPa, the turbine outlet superheats degree increases with the increases of the CO_2 temperature of the air cooler. The position of enters the constant value region moves to the direction of the increases of the high-temperature side pressure of the power cycle. It is worth noting that the turbine outlet superheat degree corresponding to the constant value is zero, indicating that the turbine outlet enters the two-phase regions, which is consistent with the phenomenon described in Fig. 19 that the condensing pressure of the power cycle finally

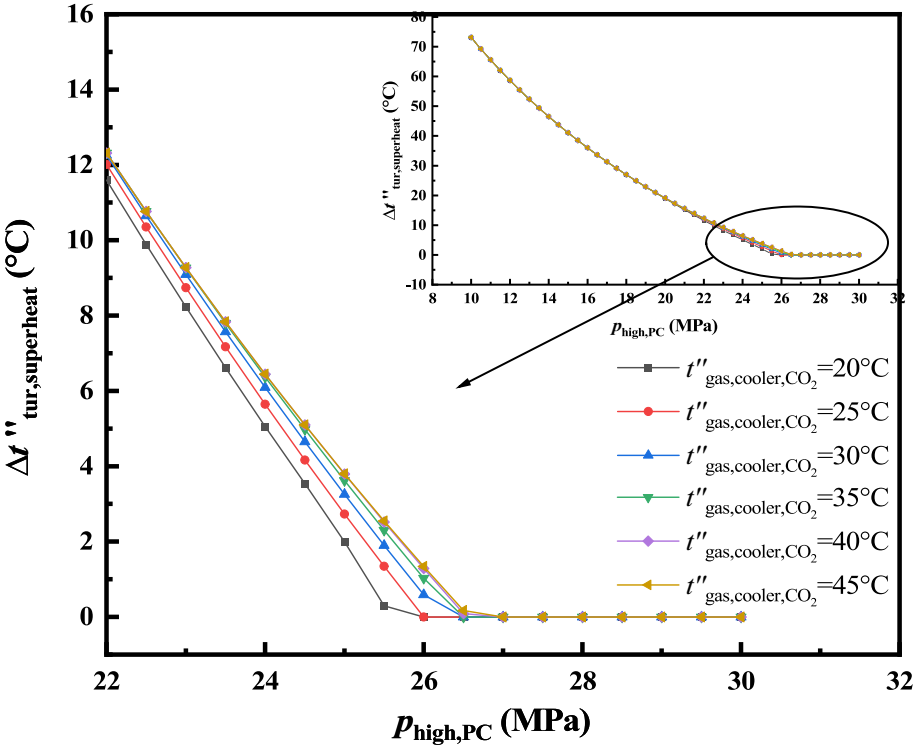

Fig. 20. Variation of turbine outlet superheat degree with high-temperature side pressure of the power cycle under different CO_2 temperatures of the air cooler outlet.

maintains a constant value with the increases of the high-temperature side pressure of the power cycle.

4. Conclusions

Based on the method of pinch point temperature difference and control variables, and the discrete treatment of high-temperature side pressure of the power cycle, the relations of operating parameters of CO_2 transcritical thermodynamic cycle energy storage system are analyzed, and the following main conclusions are summarized.

(1) The change position of the pinch point temperature difference and largest temperature difference point may lead to the curve turning.

(2) With the increases of the high-temperature side pressure of the power cycle, in general, the round-trip efficiency shows a trend of first increasing and then decreasing, and there exists a peak value, and the turbine outlet superheats degree decreases and finally keeps a constant value of zero. Therefore, the regulation of high-temperature side pressure of the power cycle is particularly important, which can not only make the round-trip efficiency of thermodynamic cycle energy storage system higher, but also avoid the turbine outlet in the two-phase regions.

(3) Decreasing the evaporating pressure of the heat pump and increasing the high-temperature side pressures of the heat pump can not only improve the peak value of the round-trip efficiency of the thermodynamic cycle energy storage system, but also the turbine outlet tends to be in the superheat region. In the calculation range, when the CO_2 temperature of the air cooler outlet is 20 °C, the peak value of round-trip efficiency is the largest, the maximum round-trip efficiency is 56.9 %. When the CO_2 temperature of the air cooler outlet increases, the CO_2 state of the turbine outlet is more inclined to the superheat region.

This investigation reveals the operating characteristics and influence mechanism of CO_2 transcritical thermodynamic cycle energy storage system, fill the gaps in relevant research, and obtain the universal rules of the energy storage system during operation. These universal rules provides a theoretical basis for the management and regulation of CO_2 transcritical thermodynamic cycle energy storage system and points out a clear direction to improve the round-trip efficiency of the system under the premise of ensuring the normal operating of the system. These universal rules may not only apply to CO_2, but also have certain guiding significance for thermal cycle energy storage systems with other substances as working fluids.

CRediT authorship contribution statement

Lisheng Pan: Conceptualization, Methodology, Investigation, Formal analysis.

Yuehua Dong: Formal analysis, Data curation, Writing – original draft.

Henglong Hao: Formal analysis, Data curation.

Xuhui Zhang: Methodology.

Weixiu Shi: Methodology.

Xiaolin Wei: Methodology.

Declaration of competing interest

The authors wish to confirm that there are no known conflicts of interest associated with this publication and all the organizations that funded the research are mentioned in the manuscript.

The authors confirm that all the persons who contributed to this paper have been mentioned as authors in the manuscript. There are no other persons who satisfied the criteria for authorship but are not listed.

Data availability

The authors do not have permission to share data.

Acknowledgments

Project 51776215 supported by National Natural Science Foundation of China is gratefully acknowledged. The authors are also grateful for the support of Beijing Natural Science Foundation (3192042).

References

[1] W. Wang, M. Zhong, L. Cheng, L. Jin, S. Shen, Forecast and analysis of the ratio of electric energy to terminal energy consumption for global energy internet, IOP Conf. Ser. Earth Environ. Sci. 121 (2018), 052061.

[2] M. Nazir, Z. Ali, M. Bilal, H. Sohail, H. Iqbal, Environmental impacts and risk factors of renewable energy paradigm—a review, Environ. Sci. Pollut. Res. 27 (27) (2020) 33516–33526.

[3] V. Henze, S. Henbest, Getting on track for net-zero by 2050 will require rapid scaling of investment in the energy transition over the next ten years, BloombergNEF (2021).

[4] H. Zhao, Q. Wu, S. Hu, H. Xu, N. Rasmussen, Review of energy storage system for wind power integration support, Appl. Energy 137 (2015) 545–553.

[5] A. Roy, S. Kedare, S. Bandyopadhyay, Optimum sizing of wind-battery systems incorporating resource uncertainty, Appl. Energy 87 (8) (2010) 2712–2727.

[6] B. Nyamdash, E. Denny, M. Malley, The viability of balancing wind generation with large scale energy storage, Energy Policy 38 (11) (2010) 7200–7208.

[7] S. Fayegh, M. Rosen, A review of energy storage types, applications and recent developments, J. Energy Storage 27 (2020), 101047.

[8] A. Arabkoohsar, in: Mechanical Energy Storage Technologies, Academic Press, 2021, pp. 1–12.

[9] K. Hodgson, Large-scale storage of electrical energy, in: Electronics and Power, 1980.

[10] S. Schoenung, Characteristics and technologies for long vs. short term energy storage, in: United States Department of Energy, Sandia report, 2001, p. 0765.

[11] S. Koohi-Fayegh, M.A. Rosen, A review of energy storage types, applications and recent developments, J. Energy Storage 27 (2020), 101047.

[12] F. Marguerite, Ueber ein neues verfahren zur speicherung elektrischer energie, Mitteilungen der Vereinigung der Elektrizitätswerke 354 (55) (1924) 27–35.

[13] R. Cahn, N. Millburn, Thermal energy storage by means of reversible heat pumping, in: United States Patent, 1978, p. 4089744.

[14] J. Hemrle, L. Kaufmann, M. Mercangoez, Thermoelectric Energy Storage System Having Two Thermal Baths and Method for Storing Thermoelectric Energy, 2009. WO2010118915.

[15] J. Hemrle, L. Kaufmann, M. Mercangoez, Thermoelectric Energy Storage System With an Intermediate Storage Tank and Method for Storing Thermoelectric Energy, 2009. WO2010145963.

[16] T. Desrues, J. Ruer, P. Marty, J. Fourmigué, A thermal energy storage process for large scale electric applications, Appl. Therm. Eng. 30 (5) (2010) 425–432.

[17] P. Vinnemeier, M. Wirsum, D. Malpiece, R. Bove, Integration of the heat pumps into thermal plants for creation of large-scale electricity storage capacities, Appl. Energy 184 (2016) 506–522.

[18] A. Koen, P. Farres-Antunez, J. Macnaghten, A. White, A low-temperature glide cycle for pumped thermal energy storage, Journal of Energy Storage 42 (2021), 103038.

[19] L. Yang, H. Li, S. Cai, L. Shao, C. Zhang, Minimizing COP loss from optimal high pressure correlation for transcritical CO_2 cycle, Appl. Therm. Eng. 89 (2015) 656–662.

[20] X. Xu, G. Chen, L. Tang, Z. Zhu, Experimental investigation on performance of transcritical CO_2 heat pump system with ejector under optimum high-side pressure, Energy 44 (1) (2012) 870–877.

[21] L. Pan, X. Wei, B. Li, T. Li, Experimental investigation on the CO_2 transcritical power cycle, Energy 95 (2016) 247–254.

[22] L. Pan, Y. Ma, T. Li, H. Li, B. Li, X. Wei, Investigation on the cycle performance and the combustion characteristic of two CO_2-based binary mixtures for the transcritical power cycle, Energy 179 (2019) 454–463.

[23] L. Pan, W. Shi, X. Wei, T. Li, B. Li, Experimental verification of the self-condensing CO_2 transcritical power cycle, Energy 198 (2020), 117335.

[24] M. Mercangöz, J. Hemrle, L. Kaufmann, A. Graggen, C. Ohler, Electrothermal energy storage with transcritical CO_2 cycles, Energy 45 (1) (2012) 407–415.

[25] M. Morandin, F. Maréchal, M. Mercangöz, F. Buchter, Conceptual design of a thermo-electrical energy storage system based on heat integration of thermodynamic cycles–part A: methodology and base case, Energy 45 (1) (2012) 375–385.

[26] M. Morandin, F. Maréchal, M. Mercangöz, F. Buchter, Conceptual design of a thermo-electrical energy storage system based on heat integration of thermodynamic cycles–part B: alternative system configurations, Energy 45 (1) (2012) 86–396.

[27] M. Morandin, M. Mercangöz, J. Hemrle, F. Maréchal, D. Favrat, Thermoeconomic design optimization of a thermo-electric energy storage system based on transcritical CO_2 cycles, Energy 58 (2013) 571–587.

[28] Y. Kim, D. Shin, S. Lee, D. Favrat, Isothermal transcritical CO_2 cycles with TES (thermal energy storage) for electricity storage, Energy 49 (2013) 484–501.

[29] Y. Baik, J. Heo, J. Koo, M. Kim, The effect of storage temperature on the performance of a thermo-electric energy storage using a transcritical CO_2 cycle, Energy 75 (2014) 204–215.

[30] F. Ayachi, N. Tauveron, T. Tartière, S. Colasson, D. Nguyen, Thermo-electric energy storage involving CO_2 transcritical cycles and ground heat storage, Appl. Therm. Eng. 108 (2016) 1418–1428.

[31] G. Wang, X. Zhang, Thermoelectric energy storage system and applications using CO_2 cycles, Energy Storage Sci. Technol. 6 (06) (2017) 1239–1249.

[32] R. Fernández, R. Chacartegui, A. Becerra, B. Calderon, M. Carvalho, Transcritical carbon dioxide charge-discharge energy storage with integration of solar energy, J. Sustain. Dev. Energy Water Environ. Syst. 7 (3) (2019) 444–465.

[33] Z. Liu, Z. Liu, X. Xin, X. Yang, Proposal and assessment of a novel carbon dioxide energy storage system with electrical thermal storage and ejector condensing cycle: energy and exergy analysis, Appl. Energy 269 (2020), 115067.

[34] Y. Zhao, C. Wang, M. Liu, D. Chong, C. Markides, J. Yan, Configuration optimization of Carnot battery energy storage system based on transcritical cycles, J. Eng. Thermophys. 42 (7) (2021) 1659–1666.

[35] D. Salomone-Gonzalez, P.L. Curto-Risso, A. Calvo Hernández, A. Medina, J.M. M. Roco, J. Gonzalez-Ayala, Pumped heat energy storage with liquid media: thermodynamic assessment by a Brayton-like model, J. Energy Storage 55 (2022), 105409.

[36] L. Pan, W. Shi, Investigation on the pinch point position in heat exchangers, J. Therm. Sci. 25 (3) (2016) 258–265.

[37] L. Pan, B. Li, W. Shi, X. Wei, Optimization of the self-condensing CO_2 transcritical power cycle using solar thermal energy, Appl. Energy 253 (2019), 113608.

[38] G. Liu, L. Ma, J. Liu, Chemistry Chemical Properties Data Manual (Inorganic Volume), Chemical Industry Press, Beijing, 2001.

[39] J. Wu, Operating Characteristics and Evaluation of NaCl Solution Crystallization System Driven by High Temperature Heat Pump, Harbin Institute of Technology, 2021.